

Hydrothermal Dissolution of Reactive Silica Materials in Sodium Hydroxide Lyes

Hallah Ahmad Alyosef[#], Bettina Lilli, Dirk Enke and Hans Roggendorf*

DOI: 10.1002/cite.202300062

 This is an open access article under the terms of the [Creative Commons Attribution-NonCommercial](#) License, which permits use, distribution and reproduction in any medium, provided the original work is properly cited and is not used for commercial purposes.



Supporting Information
available online

Reactive silica materials like vitreous silica or cristobalite were dissolved at temperatures between 100 and 220 °C for up to 7 days in NaOH lyes. The liquid and solid reaction products were analyzed chemically. Sodium water glasses with silica concentrations of up to 27 wt % and molar SiO₂/Na₂O ratios of up to 3.7 were obtained. The experimental data were evaluated by an approximation algorithm. The initial size reduction rates ranged between 0.1 and 7 μm h⁻¹, depending on the temperature and the choice of starting materials. Correlations between thermodynamics and kinetics were discussed.

Keywords: Hydrothermal dissolution, Low-quartz, Silica, Solubility, Vitreous silica, Water glass

Received: April 05, 2023; *revised:* February 14, 2024; *accepted:* June 20, 2024

1 Introduction

Alkali water glasses are produced either by melting alkaline silicate glasses and dissolving them or by dissolving quartz in alkaline lyes under hydrothermal conditions. The hydrothermal process route might offer advantages in energy consumption but is usually restricted with regard to composition and reaction times [1]. The application of SiO₂ phases with higher reactivity might improve the kinetics and widen the available composition range.

Silica or SiO₂ exists in several crystalline or amorphous phases. The phases discussed here are [2, 3]:

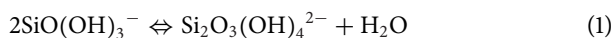
- low-quartz (or: α-quartz), the stable modification at room temperature and atmospheric pressure
- low-cristobalite (or: α-cristobalite), metastable below the phase transition to high-cristobalite
- vitreous silica

A first-order phase transition from high-cristobalite to low-cristobalite occurs at 120 to 270 °C [4]. Low-quartz is a natural material. Purer varieties are used as raw materials for water glass production. On the commercial scale, cristobalite is produced by burning low-quartz in the presence of alkalis at about 1500 °C. Vitreous silica is usually made by melting silica raw materials, by hydrolysis of SiCl₄, or by sol-gel processing [5, 6].

Commercially available sodium water glasses have compositions characterized by R_m (molar SiO₂/Na₂O ratio) values between 1.8 and 4 (R_m values of 2.0 and 3.3 are standard compositions) and silica contents of 25–35 wt %. Weldes [1] reported that R_m values up to 2.7 were reached by hydrothermal dissolution of quartz sands in sodium hydroxide lyes,

usually at temperatures of up to 200 °C. These findings were verified in [7]. Reports on the application of raw materials with a higher reactivity – like cristobalite or vitreous silica – are published in the patent literature (e.g. [8]).

The structures as well as the microstructures of water glasses were described in [9]. On the molecular scale, water glasses contain silicatic molecules like Si(OH)₄ and anions as silicatic species. Investigations by Raman and infrared (IR) spectroscopy [10] led to the conclusion that SiO(OH)₃⁻ and SiO₂(OH)₂²⁻ are the main anionic species in water glasses on the molecular scale whereas Si(OH)₄ prevails in the acidic region [5]. These anions and molecules already reflect the tetrahedral structure typical of silicates and can be regarded as monomers building up larger units by condensation reactions of the following type:



Theoretically, there is no limit to the condensation reactions. The condensed products can be regarded as polymeric silica units. The molecules can ionize in aqueous solutions. Charge compensation occurs by cations like H⁺ or R⁺

¹Hallah Ahmad Alyosef, ¹Bettina Lilli, ¹Prof. Dirk Enke,

²Prof. Hans Roggendorf (hans.roggendorf@physik.uni-halle.de)

¹Institute of Chemical Technology, University of Leipzig, 04103 Leipzig, Germany.

²Institute of Physics, Martin-Luther-University Halle-Wittenberg, Von-Danckelmann-Platz 3, 06120 Halle (Saale), Germany.

*Current address: Schüssler Novachem, 06116 Halle (Saale), Germany.

(R = Li, Na, K, ...). Water molecules can also interact with these silicatic anions to form aqueous complexes. Large molecules or colloids can be detected by light scattering [11, 12]. The term colloidal silica is usually used for stable dispersions or sols of amorphous silica [4]. In the case of water glasses, particles reaching the nanometer range can be regarded as colloids [12].

Besides trimethylsilylation [13], ^{29}Si -NMR (nuclear magnetic resonance) spectroscopy is established as the main method to characterize the molecular structure of alkaline water glasses. Different silicate anions with up to 12 silicon atoms have been detected in diluted water glasses enriched in ^{29}Si , e.g. by Harris et al. [14]. An overview on silicatic species in potassium silicate solutions has been published by Knight et al. [15]. Investigations on water glasses with compositions typical of industrial production allowed mainly the distinction of Q^n units. Q^n denotes silicon atoms connected via bridging oxygens to n ($n = 0, 1, 2, 3, 4$) other silicon atoms. Bahlmann et al. [16] made quantitative ^{29}Si -NMR measurements and showed that a sodium water glass with 30 wt % SiO_2 and $R_m = 3.4$ made by melting and dissolving a sodium silicate glass contains 0.6 % Q^0 , 4.7 % Q^1 , 29.8 % Q^2 , 50.3 % Q^3 , and 14.6 % Q^4 units. The Q^4 units and part of the Q^3 units build up colloidal silica, with Q^3 as a unit at the surface of the colloids. Roggendorf et al. [11] showed that the ^{29}Si -NMR spectra of sodium water glasses with $R_m = 2.0$ are almost independent of the method of production, whereas the respective spectra depend on the chemical composition. Matinfar and Nychka [17] recently reviewed the literature on the structure and aging of sodium silicate solutions and confirmed the findings of Bahlmann et al. [16].

The literature on the solubility of silica in general has already been reviewed by Pfeiffer et al. [7, 18, 19]. Generally, the solubility of silica increases with the pH and the temperature. At alkaline pH values, higher solubilities up to the concentration range of commercial sodium water glass compositions are reported due to the formation of negatively charged silicate ions and silica colloids [5].

The silica solubility also depends on the solid phase coexisting with the water glass. At neutral conditions (pH about 8.4), Iler [5] and Stöber [20] report that the silica solubility decreases in the order: vitreous silica > stishovite > cristobalite > tridymite > quartz > coesite.

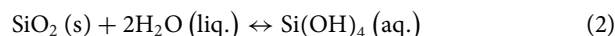
Dove and Rimstidt [21] correlated the solubility with the free enthalpy of formation of the silica phases. With respect to the dissolution behavior, amorphous silica and cristobalite are thermodynamically less stable than low-quartz in the temperature range between room temperature and 250 °C [22]. It has to be mentioned here that the term “amorphous silica” may denote different materials: dense vitreous silica as well as finely dispersed varieties such as silica gel. In citations, the original notation is used.

Iler [5] and Stumm and Morgan [23] used thermodynamic data to calculate equilibrium solubilities of low-quartz and amorphous silica involving the neutral molecule

$\text{Si}(\text{OH})_4$ as well as negatively charged silicate anions like $\text{SiO}(\text{OH})_3^-$, HSiO_3^- , and $\text{SiO}_2(\text{OH})_2^{2-}$ as a function of the pH at 25 °C. Above pH 9, the solubility of both silica phases increases due to the formation of these silicate anions. At all pH values above pH 7, the solubility of amorphous silica is by a factor of 10 higher than that of low-quartz. Thus, solubilities of amorphous silica of up to 10 mol L⁻¹ are reached.

Falcone et al. [10] confirmed the data of Stumm and Morgan [23]. They introduced the discussion on the influence of colloidal silica or higher silica oligomers on the solubility of SiO_2 .

The dissolution of silica in neutral or weakly alkaline solutions is often treated as first-order reaction, with a dissolution rate depending on the concentration. According to Rimstidt and Barnes [24], the kinetics of silica dissolution at neutral conditions is controlled by an activated transition state governing the forward and backward reactions:



In the frame of corrosion or dissolution studies on glasses or minerals, some interesting reaction models were developed. Many of these models considered – among other effects – a concentration dependence according to Noyce and Whitney [25], as already discussed in [7]. This underlying corrosion process is governed by diffusion across a boundary layer. Helgeson et al. [26] investigated the dissolution of silicate minerals. Activated sites at the surface control the dissolution kinetics. Based on the transition state theory and the linear free energy relation [27], they developed a relation between the rate and the affinity of the reaction, if other reaction variables like temperature, pressure, and surface area are kept constant:

$$\log q \propto -A \quad (3)$$

This correlation was also applied to investigate glass corrosion, as was shown by Conradt [28].

In previous studies Pfeiffer et al. [7, 18, 19] investigated the dissolution of opal, low-quartz, and technical-grade vitreous silica materials in NaOH brines under hydrothermal conditions. With opal as silica source, sodium water glasses with SiO_2 contents of up to 27 wt % and R_m of 3.4 were obtained at intermediate dissolution times [18]. At longer dissolution times, the silica concentrations decreased to about 22 wt % due to precipitation of low-quartz. Direct dissolution of low-quartz [7] revealed kinetics controlled by saturation effects and the reduction of the surface area due to dissolution of the silica grains. The surface area reduction was calculated geometrically by an iterative process. The size of the dissolving grain was reduced according to the dissolution rate as a function of the silica saturation by a term derived by Noyce and Whitney [25]. The maximal silica concentrations achieved by hydrothermal dissolution of low-quartz in NaOH lyes was solubility limited at about 20 wt % SiO_2 with R_m values of about 2.6.

Vitreous silica, which is supposed to have a higher solubility, was as source material for further dissolution tests [19]. With technical-grade vitreous silica, concentrations of 26 wt % SiO_2 and R_m values of 3.5 were reached. At low temperatures ($\leq 130^\circ\text{C}$), seeding played no role within the measuring range but the dissolution times were quite long. At higher temperatures, the dissolution kinetics were more favorable, but after a transient period of high silica concentration, the solubility of SiO_2 decreased due to seeding by impurities of low-quartz.

The investigations presented here aimed again at a water glass composition with $R_m = 3.3$ and a silica content of 25 wt % or higher. It was tried to influence the kinetics and the resulting silica contents of the water glass by choosing more reactive vitreous silica materials and by avoiding seeding effects due to impurities. These goals gain importance with increasing demand to reduce the energy consumption of chemical production. The kinetics of the dissolution process approaching saturation, the concentration limitations of the obtained water glasses, and the interaction of the kinetics and thermodynamics of hydrothermal water glass production will be discussed for the first time.

2 Experimental

2.1 Raw Materials

The following raw materials, which were supposed to have a higher purity and/or a higher reactivity, were applied:

- TECO-Sil-325F (Imerys, Greenville, USA): According to the supplier information it is a standard-grade vitreous silica powder with a median diameter of 9.3 μm and a high purity ($\text{SiO}_2 \geq 99.7$ wt %). The crystallinity was stated to be < 0.3 wt %. A scanning electron microscopy (SEM) picture is shown in Supporting Information Fig. SE2.
- TECO-Sphere A (Imerys, Greenville, USA): According to the supplier information it is a spherical vitreous silica powder with a median diameter of 15 μm of high purity ($\text{SiO}_2 \geq 99.8$ wt %). The crystallinity should be near zero. An SEM picture is shown in Supporting Information Fig. SE3.
- Quartz wool (Heraeus, Hanau, Germany): According to the supplier information it consists of vitreous silica fibers with a mean fiber diameter of 8 μm and impurities below 300 ppm (< 180 ppm Al).
- Sikron SF 3000 (Quarzwirke Group, Frechen, Germany): According to the supplier information it is a cristobalite powder with a mean diameter of 6 μm and acceptable purity ($\text{SiO}_2 = 99$ wt %; 0.2 wt % Al_2O_3 , 0.2 wt % $\text{Na}_2\text{O} + \text{K}_2\text{O}$, 0.1 wt % $\text{CaO} + \text{MgO}$, and 0.03 wt % Fe_2O_3). According to X-ray diffraction (XRD) (Fig. 1) and density [2], it is low-cristobalite.

The densities of the vitreous silica materials were measured by He pycnometry (Pycnomatic ATC; Thermo Fisher

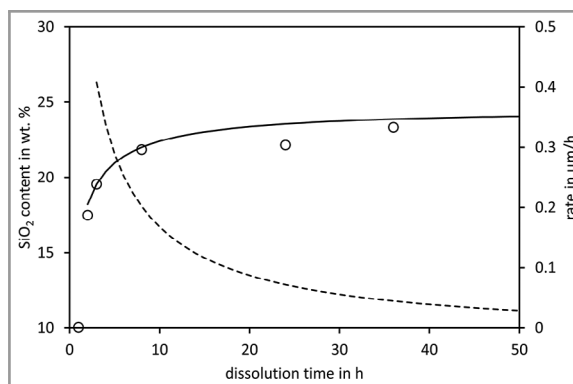


Figure 1. SiO_2 content of water glass (○) produced by hydrothermal dissolution of TECO-Sil-325F at 100°C , calculated fit of the dissolution rate (—), and dissolution rate (---) as a function of the dissolution time; batch: 10 g TECO-Sil-325F, 8.25 g NaOH lye (50 %), and 21.75 g H_2O ; $q_{\text{diss},1} = 2.0 \mu\text{m h}^{-1}$, $c_{\infty,\text{NW}} = 24.4$ wt %.

Scientific Corp., Waltham, MA, USA). Four single measurements were used to calculate mean values and standard deviations.

Chemical analysis of Sikron SF 3000 was done by X-ray fluorescence analysis (Siemens SRS 3000; Siemens, Munich, Germany, now: Bruker AXS GmbH, Karlsruhe, Germany).

The particle size distributions of the powders were analyzed by laser granulometry (CILAS 920; Quantachrome, Germany). Ultrasonic sound was used to facilitate particle separation. Particles of TECO-Sil-325F and TECO-Sphere A were investigated by SEM (LEO GEMINI 1530; Zeiss, Oberkochen, Germany). Images were taken in backscattering mode. The raw materials and some solid residues obtained in dissolution runs were characterized by XRD (URD 63, FPM Freiberg, Freiberg, Germany or STADI P, STOE, Darmstadt, Germany; $\text{CuK}\alpha$ radiation).

The silica powders were dispersed in an alkaline solution made of concentrated NaOH (AkzoNobel, Base Chemicals GmbH, Germany) diluted with deionized H_2O or with solid NaOH (pro analysis (p.a.) quality; Carl Roth, Karlsruhe, Germany) dissolved in deionized H_2O . The concentrated NaOH lye had a nominal content of 50 wt % NaOH. By titration with HCl, a value of 49.8 wt % NaOH was verified. In the case of quartz wool, solid NaOH was used as starting material for the alkaline component.

2.2 Dissolution Method

The dissolution method was described in [18]. Two different types of digestion bombs were used, each with a volume of 125 mL: polytetrafluoroethylene (PTFE)-lined steel bombs (type: Parr acid digestion bomb, bomb no. 4748; Parr Instrument GmbH, Frankfurt, Germany) for temperatures above 150°C and perfluoroalkoxy alkanes (PFA) vessels (Saville, Eden Prairie, MN, USA) for temperatures below 150°C . The digestion vessels were mounted in a rotating wheel inside

a modified cabinet dryer (WTB ED 53; Binder, Germany). The rotation speed of the bombs was 25 rpm. Dissolution temperatures between 40 and 220 °C were applied and the dissolution times ranged from 1 to 72 h. The dissolution time was corrected with respect to a dead time that is due to lower reactivity during heating and cooling. The dead times ranged between 25 and 90 min, depending on the temperature.

Due to the high thermal masses of the autoclaves (about 700 g at temperatures ≥ 160 °C and about 100 g at temperatures ≤ 160 °C) and the cabinet dryer, the lowest feasible dissolution time was 1 h.

After cooling the system down to room temperature, the resulting sample was separated by a suction filter into a liquid phase and a solid residue. A vacuum with pressures between 30 and 50 kPa was applied for nearly quantitative separation without significant evaporation of H₂O, which was proven in [7] by comparison of vacuum separated and pipetted water glasses. A round paper filter (Roth, Karlsruhe, Germany) with a retention range $> 4 \mu\text{m}$ was used.

2.3 Batch

Usually, batches of 40 g (vitreous and NaOH brine) were applied. Standard batches contained 25 wt % SiO₂ and 7.75 wt % Na₂O (the rest being H₂O), which corresponds to a molar ratio of Si₂O/Na₂O (R_m) = 3.33. Deviations from that standard batch were used to achieve higher SiO₂ solubilities and to provoke residues for XRD. Batches with SiO₂ contents of up to 33.3 wt % were applied whereas the NaOH content of the batch was not increased. Exact batches are reported in the Results section.

2.4 Analysis of the Liquid Phase

The liquid phase was titrated with 0.5 mol L⁻¹ hydrochloric acid to analyze the alkaline content (Na₂O) of the solution. Furthermore, the loss on ignition (LOI) of the liquid phase was determined in order to get the dissolved oxides or solids content in it. The samples were mixed with calcined quartz sand in order to avoid explosive steam emission during heating. Additionally, the mixture was heated stepwise via 100 and 400 °C to 900 °C, with holding times of 2 h at each temperature, and then cooled down to room temperature. The difference (LOI - Na₂O content) is equal to the silica content of the solution if impurities are neglected. The error range of this analysis was ± 0.2 wt % [7]. R_m values of the hydrothermally obtained water glasses were calculated from these data. Additionally, some samples were analyzed by inductively coupled plasma-optical emission spectrometry (ICP-OES) (Optima 8000; Perkin-Elmer, Waltham, MA, USA). This method was not applied for SiO₂ and Na₂O since dilution errors usually reduce the accuracy according to Hopp [29]. The Bastius digestion with fluoric acid

as recommended by Hopp was used for sample preparation [30].

The density (via pycnometer) and viscosity (Ubbelohde viscosimeter and/or falling ball method) were determined for selected samples.

The pH was also measured by a glass electrode (WTW pH330i, SenTixTM 41; WTW, Germany). pH measurements with glass in alkaline media are sometimes disputed because of the alkali error. Concurring methods are not precise enough (pH paper), quite complex (hydrogen electrode), or require elaborate reference systems (ion-sensitive field effect transistor). For convenience, the glass electrode was used and tested for the alkali error. The glass electrodes were calibrated with standard buffer solutions at pH 4.01, 7.01, and 10.01 (Roth, Karlsruhe, Germany). Additionally, concentrated NaOH solutions were prepared and measured. Deviations from theoretical pH values were observed above pH 12. In a 0.1 M NaOH solution, a pH of 12.7 was measured, and in a 1 M NaOH solution, a pH of 13.2, whereas below pH 12 the deviations were < 0.05 pH units. Therefore, pH values above pH 12 are not reported here. However, due to the buffer effect of sodium silicate solutions, most of the pH readings were < 12 . It might also be mentioned that concentrated sodium silicate solution significantly reduces the corrosion rates of sodium silicate glasses [31]. Therefore, no increased wear of the electrodes was observed.

The colloidal microstructure was characterized by dynamic light scattering (DLS) at a fixed angle in backscattering mode (Litesizer; Anton Parr, Ostfildern-Scharnhausen, Germany).

2.5 Analysis of the Solid Residue

The solid residues were washed with H₂O to remove alkalis, which might react with CO₂, and dried gently at 30 °C. Then, they were characterized by XRD (equipment described in Sect. 2.1).

2.6 Data Analysis

The time-dependent analytical results were evaluated with an iterative calculation procedure described in [7]: Starting with the particle size distributions (Tab. S1), the radii of the particles assumed to be spherical were reduced with an initial dissolution rate $q_{\text{diss},1}$. The volume of the dissolved particle shell was used to calculate the actual dissolved SiO₂ concentration $c_{a,u}$ (for the u -th iteration step). The iterative contribution of each dissolved particle shell was added to the mass of dissolved SiO₂. The dissolution rates were then reduced with a term according to the Noyce-Whitney law:

$$q_{\text{diss},u+1} = q_{\text{diss},u} \cdot \left(1 - \frac{c_{a,u}}{c_{\infty,NW}} \right) \quad (4)$$

$c_{\infty,NW}$ is then the final concentration value approached by the dissolution process. By optimizing $q_{\text{diss},1}$ and $c_{\infty,NW}$,

the calculated SiO_2 contents ($c_{a,u}$) are fitted to the experimentally determined SiO_2 concentrations with a least square method. The error range of $c_{\infty,\text{NW}}$ is estimated as ± 0.4 wt % (twice the value of a single measurement).

3 Results

3.1 Analysis of Raw Materials

The XRD patterns of the raw materials are displayed in Supporting Information Fig. S1. TECO-Sphere A contained minute amounts of low-quartz identified by one major peak according to a standard file of the International Center for Diffraction Data (ICDD 02-458). Supporting Information Tab. S2 compares the peak found for TECO-Sphere A and the pattern measured with Sikron SF 3000 with literature data of low-quartz and low-cristobalite.

The results of particle size analysis are listed in Supporting Information Tab. S1. The d_{50} values were: 6.9 μm (TECO-Sil-325F), 16.5 μm (TECO-Sphere A), and 4.5 μm (Sikron SF 3000). The results obtained here deviate slightly from the suppliers' information.

SEM images of TECO-Sil-325F and TECO-Sphere A are shown in Supporting Information Figs. S2 and S3. They show the different surface structures: TECO-Sil-325F has a fractured surface due to grinding whereas TECO-Sphere A has a globular appearance, which indicates formation due to surface area optimization. Nevertheless, the density measured for TECO-Sil-325F ($\rho = 2.250$ g cm^{-3}) is slightly higher than that measured for TECO-Sphere A ($\rho = 2.229$ g cm^{-3}). All densities are listed in Tab. 2.

3.2 Dissolution of Vitreous Silica Powders

Detailed results of hydrothermal dissolution with batches of TECO-Sphere A and TECO-Sil-325F are listed in Supporting Information Tabs. S3 and S4. The following observations were made with respect to the SiO_2 content:

- Temperature dependence of solution tests with TECO-Sil-325F: At temperatures of 160 and 200 $^{\circ}\text{C}$, the intended SiO_2 contents of 25 wt % were achieved with test durations of 24 h.
- Time dependence of solution tests with TECO-Sil-325F: At 100 $^{\circ}\text{C}$, a maximum of about 23 wt % SiO_2 was reached (Fig. 1). The concentration was still rising after 36 h of dissolution time. At 160 $^{\circ}\text{C}$, the total SiO_2 content of the batch was dissolved after 12 h of dissolution time (Fig. 2). The data evaluation with the iterative algorithm yielded $c_{\infty,\text{NW}} = 24.4$ wt % SiO_2 at 100 $^{\circ}\text{C}$ and $c_{\infty,\text{NW}} = 27.8$ wt % SiO_2 at 160 $^{\circ}\text{C}$. The value of $c_{\infty,\text{NW}}$ – the result of the iterative calculation – is higher than the batch content, which is thus not a limitation for the method. This shows that the cessation of the concentration increase is due to the dissolution of the complete SiO_2 content of the batch and not to the dissolution rate reduced to zero.

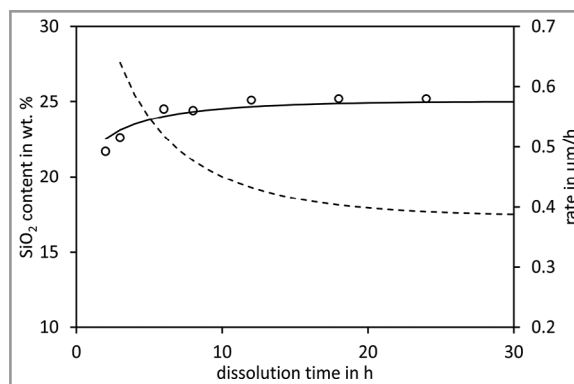


Figure 2. SiO_2 content of water glass (\circ) produced by hydrothermal dissolution of TECO-Sil-325F at 160 $^{\circ}\text{C}$, calculated fit of the dissolution rate (—), and dissolution rate (---) as a function of the dissolution time; batch: 10 g TECO-Sil-325F, 8.25 g NaOH lye (50 %), and 21.75 g H_2O ; $q_{\text{diss},1} = 3.8$ $\mu\text{m h}^{-1}$, $c_{\infty,\text{NW}} = 27.8$ wt %.

- Temperature dependence of solution tests with TECO-Sphere A: The SiO_2 contents achieved within 24 h increased with the temperature up to 160 $^{\circ}\text{C}$; at 200 $^{\circ}\text{C}$, the SiO_2 content was lower than at 160 $^{\circ}\text{C}$. This is a first hint for a precipitation at that high temperature.
- Time dependence of solution tests with TECO-Sphere A: Since the maximum SiO_2 contents in the temperature-dependent test series were achieved at 160 $^{\circ}\text{C}$, the time dependence of the dissolution of TECO-Sphere A was measured at that temperature (Supporting Information Fig. S2). The data point at the dissolution time of 8 h was treated as an outlier. With these restrictions, a $c_{\infty,\text{NW}}$ value of 24.0 wt % SiO_2 was calculated at 160 $^{\circ}\text{C}$.
 To further check these findings, additional test runs with higher SiO_2 contents of up to 27 wt % in the batches at dissolution temperatures of 160 $^{\circ}\text{C}$ (TECO-Sil-325F and TECO-Sphere A) and 200 $^{\circ}\text{C}$ (TECO-Sphere A) were made. The results are listed in Supporting Information Tab. S4. The obtained SiO_2 contents fit to those reported in Supporting Information Tab. S3. The residues of the tests were characterized by XRD. The following results were found:
 - TECO-Sil-325F at 100 $^{\circ}\text{C}$ after 48 h: One broad XRD peak is observed. The solid residue seems to be amorphous. The peak shape does also fit to cryptocrystallinity with a peak maximum at about $22^{\circ} 2\theta$. At that diffraction angle, cristobalite has its most intense peak.
 - TECO-Sil-325F at 160 $^{\circ}\text{C}$ after 48 h: Several XRD peaks that can be attributed to low-quartz and possibly to cristobalite ($28.5^{\circ} 2\theta$) together with an underlying amorphous halo are observed.
 - TECO-Sphere A at 100 $^{\circ}\text{C}$ after 48 h: An amorphous halo with a first XRD peak of low-quartz is observed. Seeding has occurred, but crystal growth is not very intense, so far.
 - TECO-Sphere A at 160 $^{\circ}\text{C}$ after 48 h: Several XRD peaks that can be attributed to low-quartz together with an underlying but faint amorphous halo are observed.

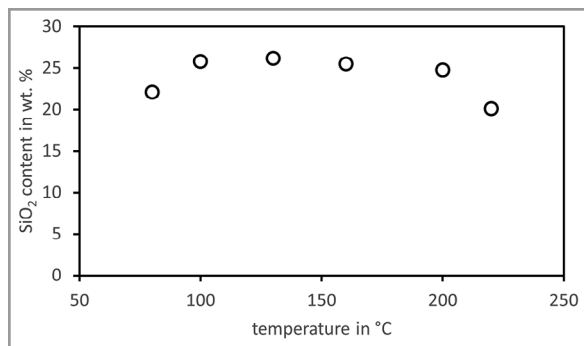


Figure 3. SiO₂ content of sodium water glasses obtained by hydrothermal dissolution of vitreous silica (Heraeus quartz wool) in NaOH lyes; batch: 4 g SiO₂, 1.6 g solid NaOH, and 10.4 g H₂O, dissolution time 48 h.

– TECO-Sphere A at 200 °C after 24 h: The observed pattern indicates almost pure low-quartz. The peaks of this XRD pattern are included in Supporting Information Tab. S2.

TECO-Sphere was more apt to crystallization. It already contained low-quartz impurities, which makes that observation plausible. Seeding and crystallization of low-quartz is improved by increasing the dissolution temperature and time.

The pH values measured after the dissolution tests started above 12 for short time tests and went down to 11.1 after longer dissolution times, reflecting the decline of free Na⁺ over time. Na⁺ is used to stabilize silicate anions and colloids. The density was raised to 1.34 g cm⁻³, which is typical of highly concentrated sodium water glasses [11]. The viscosity increased with the concentration of the sodium water glasses and reached values of 30 mPa s.

3.3 Dissolution of Quartz Wool Fibers

Detailed results obtained by hydrothermal dissolution of vitreous silica fibers are listed in Supporting Information Tab. S5. The SiO₂ contents achieved within a dissolution time of 48 h with a batch content of 25 wt % SiO₂ are shown graphically in Fig. 3 as a function of the temperature. Due to the voluminous vitreous fibers used as starting materials, the batch has to be restricted, usually to 4 g SiO₂ (about 40 % of the usual SiO₂ content). At 130 and 160 °C, the resulting experimental SiO₂ contents exceeded the batch content, probably due to evaporation of H₂O during the dissolution tests or subsequent solution treatment. At 200 and 220 °C, the resulting SiO₂ contents declined, which is taken as an indication of precipitation. Additional dissolution runs backed this finding:

- Reducing the dissolution time at 200 °C to 24 h slightly increased the SiO₂ content of the resulting sodium water glass.
- Increasing the SiO₂ content of the batch at 200 °C to 29.4 or 33.3 wt % reduced the SiO₂ content of the resulting

sodium water glass to about 20 wt %, which is close to the saturation limit of low-quartz [7]. Increasing the fiber content of the batch enlarges the exposed surface area and thus accelerates the dissolution progress, at least at the start of the dissolution process.

Since the vitreous silica fibers did not contain any crystalline impurities, seed formation during dissolution tests must have occurred at least at temperatures of 200 and 220 °C. This seeding process thus limits the silica solubility at these higher temperatures. Due to the fiber geometry, the calculation algorithm proposed in [7] was not applicable. For alternative approaches, the fiber diameter distribution has to be known (see Scholze et al. [32]), which was not measured here.

3.4 Dissolution of Cristobalite

Detailed results of dissolution tests with Sikron SF 3000 are listed in Supporting Information Tab. S6. The following results can be stated at first sight:

- Temperature dependence of dissolution for a dissolution time of 24 h: Up to 160 °C, the SiO₂ content of the resulting sodium water glass increases to 23.9 wt %. At higher temperatures, the SiO₂ content declines. XRD of solid residues (Supporting Information Tab. S6) shows the presence of low-cristobalite after dissolution runs at 100 to 160 °C. Low-cristobalite is supposed to be a remnant of the starting batch, which is incompletely dissolved. In the solid residues obtained at all five temperatures, low-quartz was detected, which is a newly formed precipitate. The intensity of the significant peak at 26.6° 2θ increases with the dissolution temperature. At 200 and 220 °C, only low-quartz was found in the solid residue. This means that the starting material of Sikron SF 3000 is completely dissolved and the solid residue is a new precipitate. Overall, the conclusion is that low-quartz precipitates and restricts the amount of dissolved SiO₂, especially at 200 and 220 °C.
- Time dependence of dissolution results obtained with batches having an intended $R_m = 3.3$ at 100 °C (Supporting Information Fig. S3) and 160 °C (Supporting Information Fig. S4): These low temperatures were chosen to avoid precipitation of low-quartz. At 100 °C, the SiO₂ content of the resulting sodium water glass approaches $c_{\infty, \text{NW}} = 24.2$ wt %, and at 160 °C, $c_{\infty, \text{NW}} = 23.9$ wt %. The determination of $q_{\text{diss},1}$ is insecure, since the calculation algorithm does not agree with the short-time results. Possibly, decrepitation of the thermally stressed cristobalite increases the surface area, thus affecting the short-time results. If that is kept in mind, the $q_{\text{diss},1}$ values at 100 and 160 °C are 0.12 and 4.2 μm h⁻¹, respectively.

3.5 Analysis of Sodium Water Glass

Samples with an increased SiO₂ content of the batch were analyzed by ICP-OES for impurities (Supporting Informa-

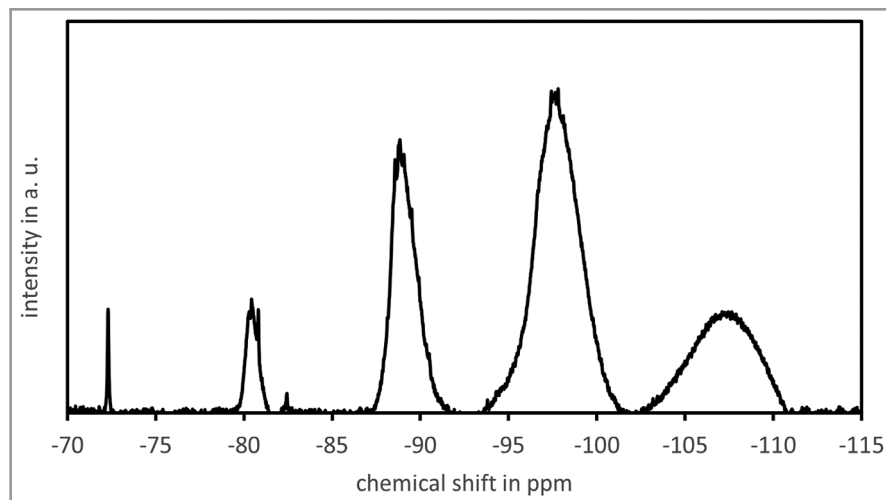


Figure 4. ^{29}Si -NMR spectrum of sodium water glass produced by dissolution of TECO-Sil-325F in NaOH lye; 25.9 wt % SiO_2 and 8.7 wt % Na_2O ; dissolution time 48 h; dissolution temperature 160 °C.

tion Tab. S4). The analysis included Al, Ca, Cu, Fe, K, and Ti. The hydrothermal treatment was performed at 160 °C for 48 h. The sample prepared with TECO-Sil-325F contained 0.02 wt % Al and 0.01 wt % Ca, and the sample prepared with TECO-Sphere A contained 0.03 wt % Al and 0.01 wt % Fe. Other elements were below the detection limits.

The ^{29}Si -NMR spectroscopy results of the samples with additional SiO_2 content (Supporting Information Tab. S4) were quite similar. The spectrum of the water glass obtained with TECO-Sil-325F at 160 °C is shown in Fig. 4; the other three spectra are displayed in the Supporting Information for comparison (Figs. S12–S14). The following six peaks were found and the band assignment is taken from Bahlmann et al. [16], who published quite similar results:

- Q^0 : (monomer) at -72.3 ppm
- Q^1 : (end group) at -80.5 ppm
- Q_3^2 : (middle group in cyclic trimers) at -82.5 ppm
- Q^2 : (middle group) at -88.8 ppm
- Q^3 : (branching group, includes surface of colloids) at -97.5 ppm
- Q^4 : (cross-linking group, includes core of colloids) at -108 ppm

The area beneath the peaks was evaluated and the results are reported in Supporting Information Tab. S7. On the molecular level, the results published so far [11, 16] are verified.

These spectra do not allow the identification of singular species, with the exception of the cyclic

trimer. If the areas under the peaks are regarded as corresponding with the concentration of the Q^n groups, the concentration of the cyclic trimer is < 0.1 %. Since core and surface groups dominate the Q^n distribution, it is concluded that the major part of the silica is present in colloidal form.

One sample of sodium water glasses obtained with batches of increased silica content was characterized by DLS. Fig. 5 shows the result obtained for TECO-Sil-325F at 100 °C. Colloidal particles with mean sizes of 1, 12, and 85 nm were found. This result is nearly identical to those published by Böschel et al. [12] for industrial sodium water glasses.

The peak at 1 nm has to be discussed. Solid silica particles with a radius of 1 nm contain about ten Si units. These particles are stabilized

by an electrostatic double layer; OH^- groups at the surface are neutralized by Na^+ . If this double layer contributes to the particle size seen by DLS, the number of Si units in the particles might be lower. On the other hand, the range of this size class goes up to 2.5 nm, which is then at least in the colloidal size range. Additionally, the NMR results indicate that the majority of the Si units are part of colloids. In [12], the particles with a diameter of about 1 nm were interpreted as primary particles, whereas the larger colloids are interpreted as secondary particles formed by aggregation of primary particles. This was concluded from the observation

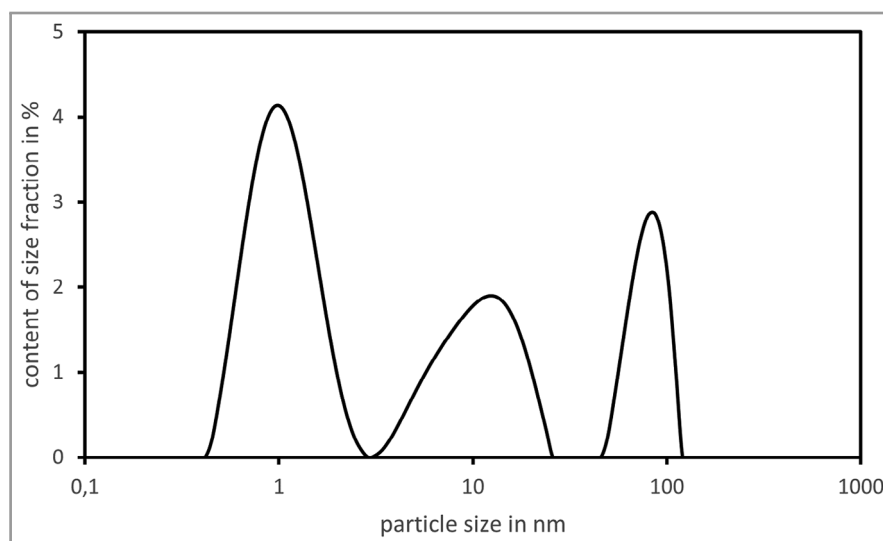


Figure 5. Particle size distribution obtained by DLS of sodium water glass produced by dissolution of TECO-Sil-325F in NaOH lye; 25.9 wt % SiO_2 and 8.7 wt % Na_2O ; dissolution time 48 h; dissolution temperature 160 °C.

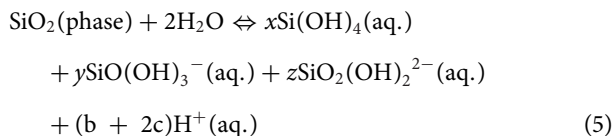
Table 1. Results of thermodynamic and kinetic analyses at temperature T for different types of silica: $q_{\text{diss},1}$, pH at 25 °C (measured) and at T (calculated), stoichiometric coefficients of Eq. (5), and free enthalpy of hydrolysis at T .

Type of silica	T [°C]	$q_{\text{diss},1}$ [$\mu\text{m h}^{-1}$]	pH at 25 °C	pH at T	x	y	z	$\Delta G_{\text{hydr},T}$ [kJ mol $^{-1}$]
TECO-Sil-325F	100	2	11.2	9.8	0.036	0.263	0.701	58.0
Sikron SF 3000	100	0.12	11.9	10.4	0.003	0.084	0.914	63.2
Vitreous silica QN-D50	100	1.46	11.4	10.0	0.018	0.197	0.785	59.0
Dörentrup W6	100	0.045	13.3	11.6	0	0.005	0.995	66.9
TECO-Sil-325F	160	3.8	11.2	9.3	0.110	0.330	0.560	62.3
TECO-Sphere A	160	6.9	11.1	9.2	0.144	0.356	0.500	60.4
Sikron SF 3000	160	4.2	11.8	9.8	0.017	0.156	0.828	71.0
Vitreous silica QN-D50	160	5.35	11.3	9.3	0.083	0.301	0.616	63.8
Dörentrup W6	160	1.04	12.3	10.2	0.003	0.067	0.930	74.5

that the respective sodium water glasses pass 25-nm filters without the loss of silica.

3.6 Thermodynamic Evaluation

Corrosion rates of five different silica materials were determined, among them were three types of vitreous silica. To establish a correlation with thermodynamics, the affinity of the dissolution reactions has to be calculated. Therefore, the free enthalpy of the following dissolution reaction was investigated:



with

$$x + y + z = 1 \quad (6)$$

Details of this thermodynamic evaluation are reported in the Supporting Information.

The dissolution rates derived for the materials investigated here and in [4] and [7], the pH values measured at the end time of the dissolution runs, and the pH values derived for reaction temperature T are listed in Tab. 1. With x , y , and z , the free enthalpies of the dissolution reaction (Eq. (5)) can be calculated with values in the range of 57–75 kJ mol $^{-1}$, which are also listed in Tab. 1.

4 Discussion

The raw materials applied here were chosen for their high reactivity in order to achieve high SiO $_2$ concentrations in short times in a technologically orientated process. The shortest feasible dissolution time of 1 h affected the kinetic evaluation especially at higher temperatures since in some

cases only few data were obtained in the time regime where the SiO $_2$ concentration increased significantly. Under these conditions, a kinetic evaluation was not possible. On the other hand, the observed higher SiO $_2$ concentration at longer dissolution times can be discussed with respect to solubility limitations. As a consequence, kinetics were compared only for results obtained at 100 °C. This shows some limitations of the applied dissolution tests.

Together with the results published in [7] and [19], a comparison between the final silica contents obtained with low-quartz, cristobalite, and different types of vitreous silica is possible. The respective results are listed in Tab. 2. The table also contains the initial dissolution rates and the measured densities of the starting materials. The following statements are found:

- Low-quartz (Dörentrup W6) [7]: An equilibrium solubility of about 20 wt % SiO $_2$ was found, which was nearly independent of the temperature. The activation energy (also Tab. 2) is 75 ± 5 kJ mol $^{-1}$.
- Low-cristobalite (Sikron SF 3000): The final silica contents of Sikron SF 3000 can be determined at dissolution temperatures of up to 160 °C by the iterative calculation process. At these temperatures, $c_{\infty, \text{NW}}$ values of about 24 wt % were reached, which is lower than the values obtained with vitreous silica varieties. At higher temperatures, the precipitation of low-quartz restricts the SiO $_2$ concentration even more. The activation energy E_A is calculated as 80 kJ mol $^{-1}$, which is comparable to the activation energy of low-quartz dissolution.
- Vitreous silica (QN-D50) [19]: The final silica contents of QN-D50 can be determined at dissolution temperatures of up to 160 °C by the iterative calculation process. At temperatures ≥ 160 °C, the maximum silica concentrations were achieved in a LaMer-type concentration development [33], which means that the liquids were oversaturated with respect to low-quartz as equilibrium component. The achieved maximum values were taken as an estimation of the solubility of vitreous silica. Values

Table 2. $c_{\infty,NW}$ and $q_{diss,1}$ values calculated for the dissolution of low-quartz Dörentrup W6 [7], vitreous silica QN-D50 [19], vitreous silica TECO-Sphere A and TECO-Sil-325F as well as of Sikron SF 3000 as a function of the temperature.^{a)}

	T [°C]	W6 [7]	QN-D50 [19]	TECO-Sphere A	TECO-Sil-325F	Sikron SF 3000
$c_{\infty,NW}$ [wt %]	100	20.5	25.8		24.4	24.2
	130	20.0	26.4			(23.6)
	160	20.1	25.5	26.8	27.8	23.9
	200	19.8	26.0 ^{b)}		(25.2)	
	220	20.5	25.5 ^{b)}		(25.3)	
$q_{diss,1}$ [$\mu\text{m h}^{-1}$]	100	0.045	1.46		2.0	0.12
	130	0.209	3.6			
	160	1.04	5.35	6.9	3.8	4.2
	200	8.0				
	220	(9.3)				
ρ [g cm^{-3}]		2.65	2.259 ± 0.001	2.250 ± 0.001	2.229 ± 0.003	2.304 ± 0.079
E_A [kJ mol ⁻¹]		76 ± 4	28 ± 5 (11)			

a) Additionally, the densities of the raw materials and (where possible) the activation energies E_A are listed; batch: 10–11 g SiO₂, 8.25 g NaOH (50 %), 21.75 g H₂O; data in brackets might have low accuracy due to insufficient data. b) c_{max} .

of $c_{\infty,NW}$ (or c_{max}) of ~ 26 wt % were obtained, again nearly independent of the dissolution temperature. QN-D50 contained already traces of low-quartz, which were detected by XRD [19] and acted as crystallization seeds at temperatures ≥ 130 °C.

- Vitreous silica (TECO-Sil-325F): This vitreous silica quality did not contain crystalline impurities, at least according to the XRD results. In prolonged dissolution tests especially at higher temperatures, seeding and crystallization of low-quartz was observed. The $c_{\infty,NW}$ values seem to increase with the temperature and reach 27.8 wt % at 160 °C; the value was calculated by the iterative calculation process with an error range of ± 0.4 wt % and was larger than the initial batch content. It was verified with a measured SiO₂ content of 27.2 wt % with increased batch content. Activation energies cannot be discussed here because of the high uncertainty of the dissolution rates observed at 160 °C.
- Vitreous silica (TECO-Sphere A): This type of vitreous silica contained low-quartz as crystalline impurities. The solubility at temperatures > 160 °C was restricted by crystallization of low-quartz. At 160 °C, $c_{\infty,NW}$ of TECO-Sil-325F was 26.8 wt % and thus slightly higher than c_{max} of QN-D50 [19]. In the time-dependent dissolution tests with TECO-Sphere A, the SiO₂ content of the batch was restricted to 25 wt %. The applied iterative calculation yielded higher $c_{\infty,NW}$ values than the batch content, but with lower accuracy. This has to be distinguished from single experiments, where evaporation during handling might slightly decrease the water content. The high solubility was verified in a dissolution test with increased SiO₂ content of the batch (= 26.8 wt %), which yielded exactly

$c_{max} = 26.8$ wt % at 160 °C. This shows that $c_{\infty,NW} = 26.8$ wt % is a realistic value. Additionally, the existence of $c_{\infty,NW}$ values showed that even the dissolution of vitreous silica, which is not considered as an equilibrium phase, approaches a temporarily metastable state, if seeding or precipitation can be avoided. In that state, either SiO₂ is totally dissolved or the rates of dissolution and precipitation of the silica phases are balanced. The $c_{\infty,NW}$ value of TECO-Sphere A at 160 °C was only 24.0 wt %, a restriction that is possibly due to precipitation induced by crystalline impurities.

- Vitreous silica (quartz wool): Due to the high fusion temperature and lower density (Tab. 2), a higher reactivity of quartz wool was expected. The SiO₂ contents at moderate temperatures reached quite high values of ≥ 25 wt %. But at temperatures ≥ 200 °C, the silica contents were again reduced by increasing temperature, dissolution time, or SiO₂ content of the batch. Although the silica precursor quartz wool did not contain crystalline impurities, crystallization occurred. Possibly, the higher reactivity enhances seed formation.

For comparison, the $c_{\infty,NW}$ values obtained at 100 °C (except for TECO-Sphere A) and 160 °C of all investigated materials are visualized in Fig. 6. The $c_{\infty,NW}$ values increased in the order low-quartz < cristobalite < vitreous silica, as already reported by Stöber [20] and Dove and Rimstidt [21] for other experimental setups. The $c_{\infty,NW}$ value of TECO-Sil-325F at 160 °C is significantly higher than the respective value obtained for QN-D50. It is possible that the QN-D50 value determined in [19] was a bit low. Then, the results obtained for TECO-Sil-325F indicate that the solubility of vitreous silica increases slightly with the

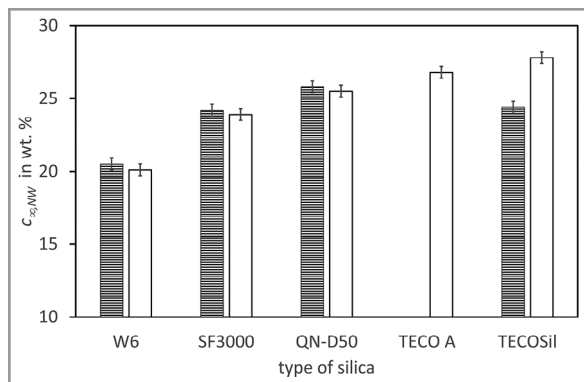


Figure 6. $c_{\infty, NW}$ values of sodium water glass produced by hydrothermal dissolution of Dörentrup W6 [7], Sikron SF 3000, QN-D50 [19], TECO-Sphere A, and TECO-Sil-325F at 100 °C (shaded rectangles) and 160 °C (empty rectangles); batch: 10 g SiO₂, 8.25 g NaOH lye (50 %), and 21.75 g H₂O; column name underlined.

temperature. Unfortunately, higher dissolution temperatures might lead to seed formation and thus to crystallization of low-quartz.

The relationship between thermodynamic calculations with a restricted data set helps to understand the limitations of hydrothermal dissolution processes for the production of sodium water glasses. The processes reach a state where dissolution and precipitation of the original phase are at equilibrium. This process is disturbed by seeding and crystallization of the thermodynamically stable low-quartz. The results on quartz indicate that even perfect glasses without crystalline impurities suffer from these effects. Possibly, their reactivity also enhances seeding. Temporarily these highly reactive silica phases allow higher silica contents of the sodium water glasses, if they are interrupted at the right time.

The temperature dependence of the kinetics was evaluated, too. Reasonable activation energies were found for the dissolution of low-quartz (W6) and low-cristobalite. The activation energies E_A for the vitreous silica varieties are rather low and are included in Tab. 2. Since only two data points of $q_{diss,1}$ as a function of the temperature were available for TECO-Sil-325F and Sikron SF 3000, no statistical error analysis was possible. Nevertheless, it can be stated that the activation energy of the dissolution of cristobalite is in the range of activation energies determined for low-quartz, whereas the activation energy of the dissolution of TECO-Sil-325F is even lower than the activation energy found for QN-D50, another type of vitreous silica investigated in [19]. An Arrhenius evaluation of the dissolution rates obtained for low-quartz and vitreous silica QN-D50 has already been reported in [19]. An equivalent diagram including the data of TECO-Sil-325F and Sikron SF 3000 is shown in Supporting Information Fig. S15. The dissolution rates of Sikron SF 3000 are a bit higher than those of

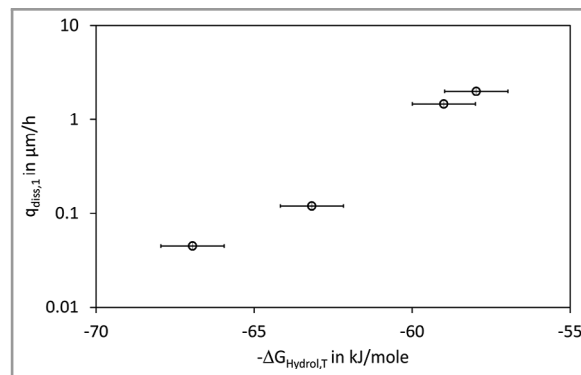


Figure 7. Relation between dissolution rate $q_{diss,1}$ and the free enthalpy of the hydrolysis reaction $\Delta G_{hydr, T}$ for the dissolution of silica varieties at 100 °C.

Dörentrup W6 but have almost the same slope. The data on vitreous silica varieties are comparable and have a lower slope. Due to the different slopes, the straight lines representing the dissolution rates of the different phases should intersect or become equal at about 220–250 °C. Therefore, it is concluded that silica phases with higher reactivity have their main advantage at lower temperatures. Regarding the demand to reduce energy consumption and CO₂ production, these reactive silica materials will gain importance in the future.

The dissolution rates determined at 100 °C were also compared with the free enthalpy of the hydrolysis reaction as determined in Sect. 3.4. The results are shown in Fig. 7 and reveal a linear free enthalpy relationship:

$$\log(q_{diss,1}) \propto -\Delta G_{hydr, T} \quad (7)$$

as proposed by Helgeson et al. [26] in Eq. (3). The coefficient of determination $R^2 = 0.99$, but one has to consider that only four data points were evaluated. The obtained relationship first allows an understanding of why silica phases follow different kinetics. A second aspect is that the relationship helps to choose raw materials for less severe and energy-intensive processes for the production of water glasses, at least if thermodynamic data are available.

Investigations on the molecular composition and the colloidal microstructure confirm the results of the literature. The ²⁹Si-NMR spectroscopy yielded results comparable to those of Bahlmann et al. [16]. Additionally, they are consistent with the finding that the conventional technological processes do not remarkably affect the molecular structure [11]. At least they do show the presence of molecular species essential for the applied thermodynamic treatment. The DLS investigations indicated a similar colloidal microstructure as proposed in [12]. Of course, more elaborate methods like two-dimensional ²⁹Si-NMR spectroscopy or dilution series in DLS might yield more detailed results but would exceed the scope of this paper.

5 Conclusion

Reactive SiO₂ qualities like vitreous silica and cristobalite in NaOH lyes under hydrothermal conditions approach transient concentration limits when dissolved under hydrothermal conditions. The resulting sodium water glasses comply with the target of this study, especially at temperatures ≤ 160 °C. At higher temperatures and longer reaction times, the precipitation of low-quartz might restrict the silica concentration. The best results were obtained with vitreous silica TECO-Sil-325F, where seeding and subsequent precipitation were retarded due to its amorphous structure without signs of crystalline impurities. Quartz wool, which was supposed to have a higher reactivity, showed solubility restrictions typical of precipitation. It is possible that high reactivity may also support seeding and precipitation. Silica contents of up to 27 wt % were reached at R_m values of 3.7, which shows that highly concentrated sodium water glasses with such a high R_m value can be obtained by hydrothermal dissolution. Comparing results for cristobalite, low-quartz, and vitreous silica types, a correlation between the dissolution enthalpy calculated with a restricted data set and the transient concentration limit was found for dissolution tests at 160 °C.

The present study shows the potential of reactive silica materials (e.g., vitreous silica) for the synthesis of sodium water glasses combining both milder conditions and comparable properties of the established products. Moreover, biogenic silica based on rice husks offers an interesting alternative, which will be the topic of an additional study.

Supporting Information

Supporting Information for this article can be found under DOI: <https://doi.org/10.1002/cite.202300062>.

[Correction added on 10 July 2024, after first online publication: Supporting Information file was updated.]

Acknowledgements

The experimental help of members of the working group Inorganic-nonmetallic Materials of the Institute of Physics of the Martin-Luther-Universität Halle-Wittenberg is gratefully acknowledged. Important contributions were provided by E. Koslowski (XRD), J. Volmer and Prof. Dr. D. Hinderberger (DLS; both Institute of Chemistry, Martin-Luther-Universität Halle-Wittenberg), Prof. Dr. J. Matysik and Dr. C. Song (²⁹Si-NMR), K. Müller (SEM), and H. Rudzik (ICP-OES; all Institute of Chemistry, University of Leipzig), which are also gratefully acknowledged.

Open access funding enabled and organized by Projekt DEAL.

Symbols used

a	[-]	activity
A	[kJ mol ⁻¹]	chemical affinity
c_a	[wt %]	actual silica concentration
$c_{a,u}$	[wt %]	actual silica concentration after $u \Delta t$
c_{\max}	[wt %]	highest measured SiO ₂ content in a test series at constant temperature
$c_{\infty,c}$	[wt %]	final SiO ₂ content due to crystallization
$c_{\infty,NW}$	[wt %]	final silica concentration according to the Noyce-Whiney law [19]
E_A	[kJ mol ⁻¹]	activation energy
$\Delta G_{\text{hydr},T}$	[kJ mol ⁻¹]	free enthalpy of hydrolysis in reaction (5)
i	[-]	number of size class
k	[s ⁻¹]	rate constant
K_a	[mol L ⁻¹]	equilibrium constant (activity)
N_A	[mol ⁻¹]	Avogadro constant
q	[mol s ⁻¹]	rate
$q_{\text{diss},l}$	[μm h ⁻¹]	initial dissolution rate
$q_{\text{diss},u}$	[μm h ⁻¹]	dissolution rate of the u -th time step
R	[J mol ⁻¹ K ⁻¹]	gas constant
R_m	[-]	molar SiO ₂ /Na ₂ O ratio
r_i	[μm]	radius of size class i
t	[h]	time
T	[K, °C]	temperature
u	[-]	number of time steps in iteration
x, y, z	[-]	stoichiometric coefficients in Eq. (5)

Greek symbols

η	[dPa s]	viscosity
λ	[nm]	wave length
ρ	[g cm ⁻³]	density
θ	[°]	diffraction angle

Sub-/superscripts

liq.	liquid
s	solid

Abbreviations

aq.	aqueous (dissolved in H ₂ O)
a.U.	arbitrary units

DLS	dynamic light scattering
LOI	loss on ignition
NMR	nuclear magnetic resonance
SEM	scanning electron microscopy
XRD	X-ray diffraction

References

- [1] H. H. Weldes, K. R. Lange, *Ind. Eng. Chem.* **1969**, *61*, 29.
- [2] R. B. Sosman, *The Phases of Silica*, Rutgers University Press, New Brunswick **1965**. DOI: <https://doi.org/10.1180/minmag.1966.035.275.19>
- [3] P. J. Heaney, in *Reviews in Mineralogy, Vol. 29, Silica* (Eds: P. J. Heaney, C. T. Prewitt, G. V. Gibbs), Mineralogical Society of America, Washington **1994**. DOI: <https://doi.org/10.1515/9781501509698>
- [4] D. M. Hatch, S. Ghose, *Phys. Chem. Miner.* **1991**, *17*, 554. DOI: <https://doi.org/10.1007/bf00202234>
- [5] R. K. Iler, *Chemistry of Silica*, Wiley-Interscience, New York **1979**. ISBN: 978-0-471-02404-0
- [6] R. Brückner, *J. Non-Cryst. Sol.* **1970**, *5*, 123. DOI: [https://doi.org/10.1016/0022-3093\(70\)90190-0](https://doi.org/10.1016/0022-3093(70)90190-0)
- [7] T. Pfeiffer, S. A. H. Sander, D. Enke, H. Roggendorf, *Chem. Ing. Tech.* **2019**, *91*, 92. DOI: <https://doi.org/10.1002/cite.201800092>
- [8] R. Novotny, A. Hoff, J. Schürtz, *German Patent DE 3902751 A1*, **1990**.
- [9] H. Roggendorf, in *Encyclopedia of Glass Science, Technology History, and Culture* (Eds: P. Richet, R. Conradt, A. Takada, J. Dyon), Wiley-VCH, Weinheim **2021**, 857. DOI: <https://doi.org/10.1002/9781118801017.ch7.5>
- [10] J. S. Falcone, J. L. Bass, P. H. Krumrine, K. Brensinger, E. R. Schenk, *J. Phys. Chem. A* **2010**, *114*, 2438. DOI: <https://doi.org/10.1021/jp908113s>
- [11] H. Roggendorf, W. Grond, M. Hurbanic, *Glastech. Ber. Glass Sci. Technol.* **1996**, *69*, 216.
- [12] D. Böschel, M. Janich, H. Roggendorf, *J. Colloid Interface Sci.* **2003**, *267*, 360. DOI: <https://doi.org/10.1016/j.jcis.2003.07.016>
- [13] K. R. Andersson, L. S. Dent Glasser, D. N. Smith, in *Soluble Silicates* (Ed: J. S. Falcone), *Am. Chem. Soc. Symp. Ser.* **1982**, *194*, 115. DOI: <https://doi.org/10.1021/bk-1982-0194.ch008>
- [14] R. K. Harris, C. T. G. Knight, *J. Chem. Soc., Faraday Trans.* **1983**, *2*, 79, 1539. DOI: <https://doi.org/10.1039/F29837901525>
- [15] C. T. G. Knight, R. J. Balec, S. D. Kinrade, *Angew. Chem. Int. Ed.* **2007**, *46*, 8148. DOI: <https://doi.org/10.1002/anie.200702986>
- [16] E. K. F. Bahlmann, R. K. Harris, B. J. Say, *Magn. Reson. Chem.* **1993**, *194*, 95. DOI: <https://doi.org/10.1002/mrc.1260310310>
- [17] M. Matinfar, J. A. Nychka, *Adv. Colloid Interface Sci.* **2017**, *7*, 76. DOI: <https://doi.org/10.1016/j.cis.2023.103036>
- [18] T. Pfeiffer, D. Enke, R. Roth, H. Roggendorf, *Adv. Chem. Eng. Sci.* **2017**, *7*, 76. DOI: <https://doi.org/10.4236/aces.2017.71007>
- [19] T. Pfeiffer, D. Enke, H. Roggendorf, *Chem. Ing. Tech.* **2021**, *93*, 473. DOI: <https://doi.org/10.1002/cite.202000107>
- [20] W. Stöber, *Beitr. Silikose-Forsch.* **1966**, *89*, 1.
- [21] P. M. Dove, J. D. Rimstidt, in *Reviews in Mineralogy, Vol. 29, Silica* (Eds: P. J. Heaney, C. T. Prewitt, G. V. Gibbs), Mineralogical Society of America, Washington **1994**, 259. DOI: <https://doi.org/10.1515/9781501509698-013>
- [22] P. Richet, Y. Bottinga, L. Denielou, J. P. Petitot, C. Tequi, *Geochim. Cosmochim. Acta* **1982**, *46*, 2639. DOI: [https://doi.org/10.1016/0016-7037\(82\)90383-0](https://doi.org/10.1016/0016-7037(82)90383-0)
- [23] W. Stumm, J. J. Morgan, *Aquatic Chemistry: Chemical Equilibria and Rates in Natural Waters*, Wiley, New York **1970**. DOI: <https://doi.org/10.5860/choice.33-6312>
- [24] J. D. Rimstidt, H. L. Barnes, *Geochim. Cosmochim. Acta* **1980**, *44*, 1683. DOI: [https://doi.org/10.1016/0016-7037\(80\)90220-3](https://doi.org/10.1016/0016-7037(80)90220-3)
- [25] A. A. Noyes, W. R. Whitney, *J. Am. Chem. Soc.* **1897**, *19*, 930. DOI: <https://doi.org/10.1021/ja02086a003>
- [26] H. C. Helgeson, W. C. Murphy, P. Aagaard, *Geochim. Cosmochim. Acta* **1984**, *48*, 2405. DOI: [https://doi.org/10.1016/0016-7037\(84\)90294-1](https://doi.org/10.1016/0016-7037(84)90294-1)
- [27] P. Atkins, J. de Paula, J. Keeler, *Atkins' Physical Chemistry*, Oxford University Press, Oxford **2018**. ISBN: 978-0-19-881789-5
- [28] R. Conradt, *J. Am. Ceram. Soc.* **2008**, *91*, 728. DOI: <https://doi.org/10.1111/j.1551-2916.2007.02101.x>
- [29] W. Hopp, *Glastech. Ber. Glass Sci. Technol.* **1993**, *66*, 1.
- [30] H. Bastius, *Fresenius Z. Anal. Chem.* **1977**, *288*, 344. DOI: <https://doi.org/10.1007/bf00433750>
- [31] M. Dathe, H. Roggendorf, *Eur. J. Glass Sci. Technol. B* **2019**, *60*, 21. DOI: <https://doi.org/10.13036/17533562.60.1.015>
- [32] H. Scholze, R. Conradt, *Ann. Occup. Hyg.* **1987**, *31*, 683. DOI: <https://doi.org/10.1093/annhyg/31.4b.683>
- [33] V. K. LaMer, *Ind. Eng. Chem.* **1952**, *44*, 1270.